

Meta-Auxiliary Learning for Micro-Expression Recognition

Jingyao Wang, Yunhan Tian, Yuxuan Yang, Xiaoxin Chen, Changwen Zheng, Wenwen Qiang*

National Key Laboratory of Space Integrated Information System

Institute of Software Chinese Academy of Sciences

University of Chinese Academy of Sciences

Beijing, China

ABSTRACT

Micro-expressions (MEs) are involuntary movements revealing people’s hidden feelings, which has attracted numerous interests for its objectivity in emotion detection. However, despite its wide applications in various scenarios, micro-expression recognition (MER) remains a challenging problem in real life due to three reasons, including (i) data-level: lack of data and imbalanced classes, (ii) feature-level: subtle, rapid changing, and complex features of MEs, and (iii) decision-making-level: impact of individual differences. To address these issues, we propose a dual-branch meta-auxiliary learning method, called LightmanNet, for fast and robust micro-expression recognition. Specifically, LightmanNet learns general MER knowledge from limited data through a dual-branch bi-level optimization process: (i) In the first level, it obtains task-specific MER knowledge by learning in two branches, where the first branch is for learning MER features via primary MER tasks, while the other branch is for guiding the model obtain discriminative features via auxiliary tasks, i.e., image alignment between micro-expressions and macro-expressions since their resemblance in both spatial and temporal behavioral patterns. The two branches of learning jointly constrain the model of learning meaningful task-specific MER knowledge while avoiding learning noise or superficial connections between MEs and emotions that may damage its generalization ability. (ii) In the second level, LightmanNet further refines the learned task-specific knowledge, improving model generalization and efficiency. Extensive experiments on various benchmark datasets demonstrate the superior robustness and efficiency of LightmanNet.

CCS CONCEPTS

• Computing methodologies → Transfer learning; Computer vision tasks; • Information systems → Sentiment analysis.

KEYWORDS

micro-expression recognition; few-shot learning; meta-auxiliary learning; emotion recognition

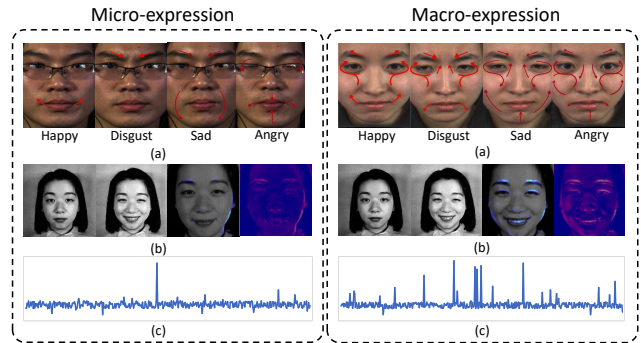


Figure 1: Comparison of micro- and macro- expressions. (a) shows examples of different expressions, where the red arrow represents the muscle movement direction. (b) shows the optical flow of expressions in a “happy” video sequence, where the highlight indicates the movement area. (c) shows the change in amplitude of the receptive fields of different expressions, where the spikes indicate that the pixel changes are high. More details are provided in the Appendix.

1 INTRODUCTION

Micro-expressions (MEs) are involuntary facial movements that are highly associated with human mental states, attitudes, and intentions [34]. These fleeting expressions offer glimpses into people’s genuine feelings even in high-stakes situations, making them one of the most powerful and objective tools for understanding human psychology. The practical importance of micro-expression recognition (MER) has been demonstrated in various fields, e.g., healthcare [22], criminal interrogation [36], and intelligent marketing [67].

Early methods for MER relied heavily on conventional features [11, 14, 19]. Recently, with the success of deep learning in various scenarios, neural networks have received increasing interest in MER [3, 24, 29]. However, despite its wide applications in some fields, e.g., criminal investigations and clinical interactions involving autistic patients [5, 33], automatic micro-expression recognition remains a challenging problem in real-world applications for three reasons: (i) data-level: lack of data and imbalanced classes, (ii) feature-level: subtle, rapid changing, and complex features, and (iii) decision-making-level: impact of individual differences.

Specifically, MEs are spontaneous and unplanned facial expressions revealing people’s hidden feelings in high-stakes situations when people try to conceal their true feelings, making collecting and annotating data challenging. Existing publicly available datasets are often small in size [57, 71], and struggle to meet the supervised paradigm’s reliance on large amounts of continuously annotated data.

Permission to make digital or hard copies of all or part of this work for personal or classroom use is granted without fee provided that copies are not made or distributed for profit or commercial advantage and that copies bear this notice and the full citation on the first page. Copyrights for components of this work owned by others than the author(s) must be honored. Abstracting with credit is permitted. To copy otherwise, or republish, to post on servers or to redistribute to lists, requires prior specific permission and/or a fee. Request permissions from permissions@acm.org.

ACM MM, 2024, Melbourne, Australia

© 2024 Copyright held by the owner/author(s). Publication rights licensed to ACM.

ACM ISBN 978-x-xxxx-xxxx-x/YY/MM

<https://doi.org/10.1145/nnnnnnn.nnnnnnn>

Next, we turn to the features and find that different from macro expressions, MEs are spontaneous, subtle, and rapid (1/25 to 1/3 second) facial movements reacting to emotional stimulus [8, 26], making learning more challenging. Figure 1 shows examples of micro- and macro-expressions, as well as facial optical flow motion and response signal under a set of emotional clips. We also provide the results including optical flow maps and dynamically changing regions. The frame where facial movement begins is denoted as the start frame, while the end frame is denoted as the offset frame, and the frame with the greatest intensity is the vertex frame. More details are provided in Appendix C. From the results, we can observe that micro-expressions have short duration and low action intensity, making their learning more challenging. In addition, MEs can also be impacted by emotional context and cultural background [34, 65], with individual differences. For example, some people express happiness more by raising the corners of their mouths, while others express happiness by raising their eyebrows. Therefore, MER still faces great challenges in practical applications.

To address the above issues, an ideal MER model needs to accomplish three key objectives: (i) extracting discriminative features of MER from limited data; (ii) capturing rapidly changing and imperceptible features, including the amplitude and direction of expressions, while preventing extracting noise or redundant features; (iii) acquiring general MER-related knowledge to accommodate individual differences in emotional expression.

Based on this insight, in this paper, we propose a dual-branch meta-auxiliary learning method, called LightmanNet, for robust and fast micro-expression recognition. Specifically, LightmanNet first reconstructs the MER tasks through random sampling from limited data, wherein each task encompasses distinct knowledge with both micro-expressions and macro-expressions. Subsequently, it divides these tasks into two branches: the first branch for model decision-making, handling the primary MER task, while the second branch aids in training guidance, dealing with auxiliary tasks of image amplification and alignment. These auxiliary tasks consider the similar spatial and temporal behavioral patterns between micro-expressions and macro-expressions. It aids the model in extracting more meaningful representations, steering clear of learning superficial connections that might compromise its ability to generalize. Finally, LightmanNet employs bi-level optimization to acquire general knowledge from learning in both branches, facilitating accurate MER. In summary, LightmanNet addresses the above three issues through a dual-branch bi-level optimization process, and its outstanding performance is demonstrated through extensive experiments. The contributions are as follows:

- We are the first to explore all three key challenges of micro-expression recognition in real-life multimedia applications, including data level, feature level, and decision-making level.
- We propose a novel dual-branch meta-auxiliary learning method, called LightmanNet, to achieve robust and fast micro-expression recognition. It enables the model to quickly obtain discriminative and general MER-related knowledge from limited data, improving model generalization and efficiency.
- Extensive experiments conducted on multiple benchmark datasets demonstrate the outstanding robustness and effectiveness of the proposed LightmanNet.

2 RELATED WORK

2.1 Micro-expression Recognition

Micro-expression recognition is an important technology for facial expression analysis and sentiment analysis in real-life multimedia applications. This technology focuses on capturing short and subtle facial expression changes and discovering hidden emotional information and psychological states. It has been widely used in various fields, such as medical diagnosis [22], interpersonal communication [67], false information detection [36], etc., providing richer information and deeper insights [22, 36, 67]. Existing MER methods mainly can be divided into two categories, i.e., traditional MER methods and deep learning-based MER methods.

Traditional MER methods, e.g., optical flow and local binary pattern, usually analyze micro-expression features based on features, e.g., color, texture, etc. [11, 14, 19]. Liu et al. [32] proposed a directional mean optical-flow feature with a Support Vector Machine classifier for MER. Liong et al. proposed bi-weighted oriented optical flow as a new feature extractor [30]. Zhao et al. [69] applied local binary pattern-three orthogonal planes and a block-based method to analyze dynamic texture features of input images.

Deep learning-based MER methods mainly use deep neural networks for feature extraction and emotion recognition [24, 29]. Zhai et al. [66] proposed a self-supervised generation module to calculate the displacement of frames, utilizing a Transformer Fusion mechanism to extract features from onset-apex pairs. Nguyen et al. [38] focused on interest regions of MER by detecting the differences between micro-expressions of two frames. Xia et al. [60] propose a macro-to-micro transformation framework for micro-expression recognition, which pre-trains the model both with micro-expression data and macro-expression data respectively.

However, although existing methods have achieved good results, they rely on a large amount of continuous and pure data while ignoring three key challenges in the real-world MER applications as mentioned in Section 1. In this study, we aim to explore and solve all three key challenges of real-life MER.

2.2 Meta-Learning

Meta-learning, also known as “learning to learn”, attempts to adapt to new environments rapidly with limited data. The meta-learning methods can be divided into three types, including optimization-based, model-based, and metric-learning-based methods.

Optimization-based methods aim to acquire a set of optimal initialization parameters that facilitate rapid convergence when confronted with new tasks. Key methodologies in this category encompass MAML [10], Reptile [40], and ANIL [45]. MAML trains a model capable of adapting to diverse tasks by sharing initial parameters across different tasks and executing multiple gradient updates. Similarly, Reptile shares initial parameters but employs an approximate update strategy, wherein the model undergoes fine-tuning through multiple iterations to approach optimal parameters.

Model-based methods perform the optimization process in a single model. The classic methods include recurrent networks [46], convolutional networks [16], memory-augmented neural networks [48], and hypernetworks [12, 43] that embed training instances and labels of training tasks to define a predictor for test samples. In contrast to optimization-based methods, these methods offer

simpler optimization procedures that do not necessitate second-order gradients. Nonetheless, there is a noted tendency for them to exhibit less robust generalization to tasks outside their trained distribution. Although they excel in few-shot learning scenarios, criticisms have arisen regarding their asymptotic performance [17].

Metric-learning-based methods focus on acquiring embedding functions that map instances from distinct tasks. These functions facilitate easy classification through non-parametric methods. This concept has been investigated by various approaches, which vary in their approaches to learning embedding functions and distance metrics within the feature space. The influential methods include ProtoNet [50], RelationNet [52], and MatchingNet [54]. They aim to solve problems by learning a shared embedding space and amortizing inference, where classification can be performed by calculating distances to prototype representations.

Recently, there have been studies using meta-learning to solve the problem of data scarcity in MER. Wan et al. [55] directly use MAML for micro-expression recognition. Gong et al. [13] proposed a meta-learning-based multi-model fusion network (Meta-MMFNet) to solve the existing challenging problem of the lack of training data. However, they only use meta-learning on few-shot MER scenarios under ideal conditions (i.e., relying on pure data), which may contain redundant features and noise. Despite some research [2, 4, 39] also focused on few-shot MER, aiming to solve data-level problems, they also ignored the feature-level and decision-making-level challenges that exist in real applications as mentioned above. In this paper, We aim to propose a general framework to solve three key challenges of real-life MER, making the model obtain discriminative and generalizable MER features.

3 PRELIMINARY

Meta-learning, also known as learning to learn, seeks to bootstrap learning capabilities from a pool of tasks in order to accelerate the learning process when faced with a new task. These tasks are assumed to originate from a predetermined distribution $p(\tau)$, represented as $\tau \sim p(\tau)$. During the meta-training phase, N tasks denoted as $\mathcal{D}_{tr} = \{\tau_i\}_{i=1}^N$ are randomly selected from this distribution, and datasets associated with these tasks become available to the learner. Each task τ_i consists of a support set $\mathcal{D}_i^s = (X_i^s, Y_i^s) = \{(x_{i,j}^s, y_{i,j}^s)\}_{j=1}^{N_i^s}$ and a query set $\mathcal{D}_i^q = (X_i^q, Y_i^q) = \{(x_{i,j}^q, y_{i,j}^q)\}_{j=1}^{N_i^q}$. Note that each sample $x_{i,j}^s$ is a video sequence containing M frames. In this paper, we propose introducing auxiliary tasks, i.e., image alignment between micro-expressions and macro-expressions, to guide model learning MER-related knowledge. Thus, given that our study encompasses two categories of tasks, we encounter N additional auxiliary tasks $\tau^{aux} \sim p(\mathcal{T})$, each accompanied by multiple smaller datasets $\{\mathcal{D}_i^{aux}\}_{i=1}^N$. Meta-learning strives to construct a model f_θ using the collective knowledge from the $2N$ training tasks (N primary tasks and N auxiliary tasks). The model f_θ is designed in a manner that enables rapid adaptation and minimization of training loss when presented with a given task.

For the learning paradigm, take the most commonly used MAML [10] as an example, it accomplishes this by acquiring initial parameters θ , which involves executing a few iterations of gradient descent starting from θ utilizing the training tasks. Take the vanilla

framework as an example, the model f_θ is optimized only based on the N training tasks of the main branch without the guidance of auxiliary tasks. To obtain this starting point, MAML addresses the optimization problem:

$$\begin{aligned} & \arg \min_{f_\theta} \frac{1}{N} \sum_{i=1}^N \mathcal{L}(\mathcal{D}_i^q, f_\theta^i), \\ & \text{s.t. } f_\theta^i = \arg \min_{f_\theta} \mathcal{L}(\mathcal{D}_i^s, f_\theta), \end{aligned} \quad (1)$$

where α is the learning rate, f_θ^i is the task-specific model obtained by taking the derivative of the meta-learning model f_θ , $\mathcal{L}(\mathcal{D}_i^s, f_\theta)$ is the training loss of the task-specific model f_θ^i on the support set, $\mathcal{L}(\mathcal{D}_i^q, f_\theta)$ is the loss of the trained f_θ^i on the query set. Thus, the optimization process of the meta-learning f_θ can be viewed as calculating the second derivative of f_θ .

4 METHOD

In this section, we present the proposed method, LightmanNet, for micro-expression recognition. We first introduce the model architecture of LightmanNet in Subsection 4.1, which has a two-branch architecture that jointly solves two related tasks. Given a sequence of observed frames, the primary task aims to recognize the emotions contained in the micro-expressions of these frames. In addition to the primary branch, LightmanNet has another branch that solves an auxiliary task complementary to the primary task, i.e., image alignment. These two tasks share the backbone features and can be jointly learned. Next, we introduce the learning details of LightmanNet in Subsection 4.2, which is a dual-branch bi-level optimization process of meta-auxiliary learning. Figure 2 provides an overview of our approach. The pseudo-code is shown in Algorithm 1.

4.1 Model Architecture

As shown in Figure 3, LightmanNet has a dual-branch structure. The network takes multiple consecutive video frames as input, and we denote the M frames of each input video sequence as $\{I_i\}_{i=1}^M$. The main branch extracts the emotions from micro-expressions in the video sequences. The auxiliary branch contains image alignment tasks between micro-expressions and macro-expressions for their resemblance in both spatial and temporal behavioral patterns.

These two branches share the same 2DCNN backbone network for feature extraction, which can be any image classification network, e.g., Conv4 [10], VGG-19 [49], ResNet [15], and DenseNet [18]. To save computation, we use the simple and lightweight Conv4 with the last fully convolutional layer removed as our backbone. Then, we combine a 3DCNN network [68] to encode the multiple-frame features of the last convolutional layer of the backbone network, and use a single 3D convolutional layer with kernel size 6 along the time dimension. The 3DCNN module can capture the temporal information in the video sequences. Finally, we design the decoder following [31, 47], when it upsamples the features from low resolution to input resolution, a convolutional layer is added to output three different scales of the feature maps. We explain the two branches in more detail below.

Primary Task Learning. We use a commonly used classification loss, i.e., cross-entropy loss [7], to constrain the learning of the

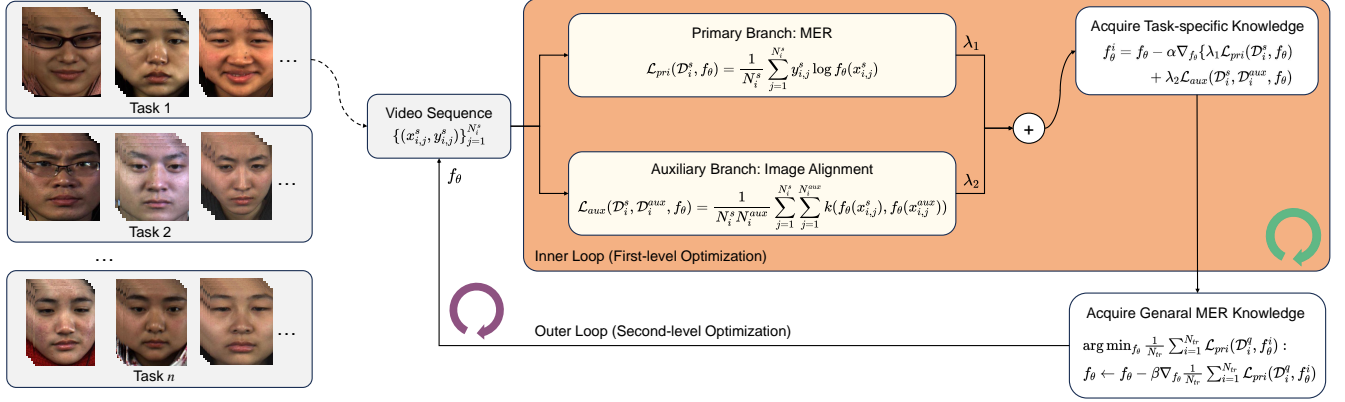


Figure 2: Overview of LightmanNet. It first builds various training tasks (gray boxes on the left), and then learns general MER-related knowledge via bi-level optimization: (i) in the first level (green circle), the model f_{θ} learns task-specific MER knowledge for task τ_i and obtain f_{θ}^i through two branches of learning, i.e., $f_{\theta} \rightarrow f_{\theta}^i$, where the primary branch is used to learn MER features, while the auxiliary branch is used to guide f_{θ} to obtain discriminative features; then, (ii) in the second level (purple circle), f_{θ} refines the learned task-specific knowledge of f_{θ}^i , i.e., optimized with the cumulative loss of multiple f_{θ}^i .

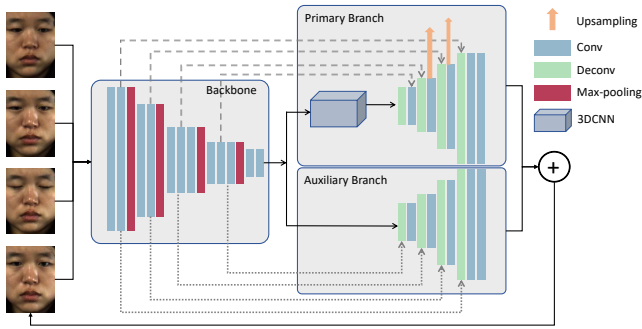


Figure 3: Illustration of our model architecture. The two branch structures of the model share the same 2DCNN network for feature extraction (left side), but the last layer of the encoder and the decoder are different (right side).

main task (MER tasks) branch:

$$\mathcal{L}_{pri}(\mathcal{D}_i^s, f_{\theta}) = \frac{1}{N_i^s} \sum_{j=1}^{N_i^s} y_{i,j}^s \log f_{\theta}(x_{i,j}^s), \quad (2)$$

where $\mathcal{L}_{pri}(\tau_i)$ is the loss for the primary MER task τ_i , \mathcal{D}_i^s is the support set of task τ_i , f_{θ} is the learning model.

Auxiliary Task Learning. Learning a primary task alongside a proper auxiliary task can force the model to capture more meaningful representations, steering clear of learning superficial connections that might compromise its ability to generalize [31, 37]. The auxiliary task should be selected wisely to support the primary task, or else the primary task’s performance will deteriorate. We need an auxiliary task that can teach the network how to recognize subtle, dynamic, and complex ME features.

In this paper, we propose to use image alignment [53, 60] as the auxiliary task. Image alignment is performed since micro-expression and macro-expression share some similarities in both spatial and

temporal behavior patterns. To perform well in this task, the model needs to learn feature representations that capture the geometric and semantic information of the scene, which intuitively will be useful for efficient MER as well.

We design the image alignment branch similar to the MER decoder based on the shared feature encoder. In this branch, we evaluate the feature alignment degree of micro-expressions and macro-expressions by measuring Maximum Mean Discrepancy (MMD). Given the support set \mathcal{D}_i^s of the main task τ_i and the support set \mathcal{D}_i^{aux} of the auxiliary task τ_i^{aux} , the loss can be expressed as:

$$\mathcal{L}_{aux}(\mathcal{D}_i^s, \mathcal{D}_i^{aux}, f_{\theta}) = \frac{1}{N_i^s N_i^{aux}} \sum_{j=1}^{N_i^s} \sum_{k=1}^{N_i^{aux}} k(f_{\theta}(x_{i,j}^s), f_{\theta}(x_{i,k}^{aux})), \quad (3)$$

$$s.t. \quad k(x, y) = \exp\left(-\frac{\|x-y\|^2}{2\sigma^2}\right),$$

where N_i^s and N_i^{aux} are the number of samples in tasks τ_i and τ_i^{aux} , \mathcal{D}_i^s and \mathcal{D}_i^{aux} are the support sets of tasks τ_i and τ_i^{aux} , and $k(\cdot, \cdot)$ is the Gaussian kernel function.

4.2 Meta-Auxiliary Learning

To effectively extract valuable knowledge from limited data, LightmanNet utilizes a bi-level optimization for meta-auxiliary learning. This approach enables the acquisition of general knowledge from both branches, thereby enhancing accurate Micro-Expression Recognition (MER). Specifically, LightmanNet first extracts micro-expression features from the limited data of each task through joint training on two branches, facilitating the acquisition of meaningful knowledge. Subsequently, LightmanNet employs knowledge distillation on the acquired knowledge to further enhance the model’s generalization capability.

Formally, The goal of LightmanNet is to learn the parameters θ of the model f_{θ} so that they can be effectively used for adaptation. The model f_{θ} is divided into three parts as shown in Figure 3, expressed as $f_{\theta} = g \circ \{h_{pri}, h_{aux}\}$, where g represents the backbone network, h_{pri} and h_{aux} denote the primary MER branch and the

Algorithm 1 Pseudo-Code of LightmanNet

Require: The primary tasks \mathcal{D}_{tr} ; the auxiliary tasks \mathcal{D}^{aux} ; meta-auxiliary learning model f_θ ; The hyperparameter λ_1 and λ_2 ; Learning rates α and β

for all τ_i **do**

Obtain support sets and query sets for both the primary MER task and the auxiliary task

Calculate primary task loss \mathcal{L}_{pri} via Eq.2

Calculate auxiliary task loss \mathcal{L}_{aux} via Eq.3

Update the task-specific model f_θ^i via 4

end for

Update the model f_θ via Eq.4

return solution

auxiliary image alignment branch, respectively. In the first level optimization, f_θ aims to learn task-specific knowledge by minimizing the losses \mathcal{L}_{pri} and \mathcal{L}_{aux} in Eq.2 and Eq.3 over tasks τ_i and τ_i^{aux} of both the branches. Then, in the second level optimization, f_θ is updated based on the cumulative loss of multiple groups of tasks, that is, acquiring general knowledge distilled from the acquired task-specific knowledge. The objective of LightmanNet becomes:

$$\arg \min_{f_\theta} \frac{1}{N_{tr}} \sum_{i=1}^{N_{tr}} \mathcal{L}_{pri}(\mathcal{D}_i^q, f_\theta^i), \quad (4)$$

$$s.t. \quad f_\theta^i = \arg \min_{f_\theta} \lambda_1 \mathcal{L}_{pri}(\mathcal{D}_i^s, f_\theta) + \lambda_2 \mathcal{L}_{aux}(\mathcal{D}_i^s, \mathcal{D}_i^{aux}, f_\theta),$$

where N_{tr} denotes the number of training tasks, λ_1 and λ_2 are the weights of the losses \mathcal{L}_{pri} (Eq.2) and \mathcal{L}_{aux} (Eq.3) over tasks τ_i and τ_i^{aux} , f_θ^i is the task-specific model obtained by taking the derivative of the model f_θ . The learning rates of the first-level and second-level objectives are α and β , respectively. It is worth noting that the auxiliary task is used to guide the model to extract complex micro-expression features and does not involve the acquisition of general knowledge, i.e., the second-level optimization.

Through the above process, we obtained the final model f_θ which can quickly adapt to any task well with limited data. In the testing phase, for any unseen MER task τ_{te} , f_θ is first fine-tuned on the data set (usually only 1 step is required) to quickly extract task-specific MER knowledge And get f_θ^{te} . Finally, we process the unseen video data in the test task based on the model f_θ^{te} to obtain accurate MER results. Therefore, LightmanNet well eliminates the effects of lack of samples, complex features, and individual differences, and its generalization and robustness will be verified in Section 5.

5 EXPERIMENTS

In this section, we first introduce the experimental settings in Subsection 5.1. Then, we present the comparative experiments between our method and the baselines from two aspects: performance and model efficiency in Subsection 5.2. Next, we analyze the robustness of our approach in Subsection 5.3, which reflects the effect of the proposed method when lack of data and differences between classes. Furthermore, we perform ablation studies to further explore how LightmanNet works in Subsection 5.4. All results are averaged over five rounds of testing. More details and additional experiments are provided in the Appendix.

5.1 Experimental Settings

In this subsection, we introduce the datasets, baselines, implementation details, and evaluation metrics in sequence.

Datasets. We select five MER benchmark datasets, including (i) SAMM dataset [6] which contains 159 micro-expression clips from 32 participants; (ii) SMIC dataset [28] that consists of 164 micro-expression samples from 16 subjects; (iii) CASME dataset [64] that contains 195 micro-expression videos sampled from 19 individuals; (iv) CASME II [63] that expands on the CASME and contains five emotions; and (v) CAS(ME)² dataset [44] includes both macro-expressions and micro-expressions, categorizing emotions into three groups: positive, negative, and surprise, and be further divided into 12 detailed emotional labels, i.e., happiness, sadness, fear, surprise, anger, disgust, trust, hate, contempt, guilt, grateful, and bittersweet [25, 41, 56]. Meanwhile, we use the Composite Database Evaluation (CDE) which combines samples from all datasets together into a single database to evaluate the performance of our proposed LightmanNet following [39]. For auxiliary tasks construction, we use the CK+ database as the macro-expression database following [60]. More details are shown in Appendix A.

Baselines. We extensively compare LightmanNet with four types of baselines for comprehensive evaluation, including (i) traditional MER methods [13] including LBP-TOP [23], LBP-SIP [58], STLBP-IP [19], STCLQP [20], HIGO [27], FHOFO [14] and Bi-WOOF [30]; (ii) deep-learning-based MER methods [39] including OFF-Apex [11], Boost [42], DSSN [21], AU-GACN [62], Dynamic [51], MicroNet [61], Graph-TCN [24], MiMaNet [60], FR [70], AMAN [59], SelfME [9], μ -BERT [39] and FRL-DGT [66]; (iii) meta-learning methods mentioned in Subsection 2.2, e.g., MAML [10], Reptile [40] and ANIL [45]; and (iv) meta-learning-based MER methods including MEReMAML [55] and Meta-MMFNet [13]. These baselines cover the SOTA baselines and classic MER methods for each benchmark dataset. More baselines are provided in Appendix B.

Implementation Details. We choose the Conv4 backbone for the encoder and the overall structure is illustrated in Subsection 4.1. Following the convolution and filtering stages, we apply batch normalization, ReLU non-linear activation, and 2×2 max pooling in sequence. The output of this encoder consists of two separate branches, i.e., the primary branch and the auxiliary branch. The construction of training tasks of each dataset or domain follows the process mentioned in Section 3. Moving to the optimization stage, we employ the Adam optimizer with momentum and weight decay values set at 0.9 and 10^{-4} . The initial learning rates, i.e., α and β mentioned in Eq.4, for all experiments are established at 0.2 and 0.1, with the option for linear scaling as required. All experiments are conducted on 10 NVIDIA V100 GPUs.

Evaluation Metrics. We select five commonly used metrics for evaluation, including (i) accuracy (%) which is a commonly used metric to evaluate the overall performance of a classification model; (ii) F1 score (%) which combines precision and recall into a single value; (iii) unweighted average recall (UAR) (%) which computes the average recall across all classes without considering the class imbalance; (iv) training time (h) which is used to evaluate the model efficiency; and (v) model size (M) refers to the amount of memory

Table 1: Performance (accuracy & F1 score \pm 95% confidence interval) of baselines and LightmanNet on the datasets mentioned in Subsection 5.1. All results are provided in the corresponding papers or are obtained based on the source code. Note that the meta-learning-based baselines follow the few-shot settings mentioned in Subsection 5.3. The “-” denotes that the result is not reported, and the best results are highlighted in bold. See Appendix C for full results.

Method	SAMM(CK+)		SMIC(CK+)		CASME(CK+)		CASME II(CK+)		CAS(ME) ² (CK+)	
	ACC	F1								
LBP-TOP	59.23 \pm 0.35	36.40 \pm 0.42	58.80 \pm 0.35	60.05 \pm 0.41	57.11 \pm 0.49	58.02 \pm 0.45	49.00 \pm 0.53	51.01 \pm 0.34	-	-
LBP-SIP	41.56 \pm 0.51	40.60 \pm 0.51	44.53 \pm 0.52	44.92 \pm 0.34	43.42 \pm 0.36	45.30 \pm 0.34	46.53 \pm 0.47	44.82 \pm 0.48	-	-
STLBP-IP	56.82 \pm 0.38	52.73 \pm 0.40	57.96 \pm 0.35	58.00 \pm 0.36	56.72 \pm 0.29	57.92 \pm 0.53	59.53 \pm 0.35	57.02 \pm 0.32	51.73 \pm 0.42	52.33 \pm 0.38
STCLQP	63.82 \pm 0.32	61.11 \pm 0.41	58.31 \pm 0.35	58.38 \pm 0.51	57.31 \pm 0.32	56.02 \pm 0.27	64.10 \pm 0.33	63.88 \pm 0.37	56.31 \pm 0.33	56.87 \pm 0.32
HIGO	-	-	68.20 \pm 0.33	67.5 \pm 0.33	61.52 \pm 0.33	63.20 \pm 0.34	-	-	58.26 \pm 0.34	58.10 \pm 0.28
FHOFO	-	-	51.89 \pm 0.40	52.34 \pm 0.42	67.01 \pm 0.29	54.92 \pm 0.34	56.60 \pm 0.34	52.49 \pm 0.33	48.93 \pm 0.25	47.92 \pm 0.30
Bi-WOOF	58.30 \pm 0.36	39.72 \pm 0.49	62.22 \pm 0.33	62.00 \pm 0.29	69.42 \pm 0.38	69.8 \pm 0.23	58.87 \pm 0.36	61.10 \pm 0.36	50.62 \pm 0.33	51.30 \pm 0.34
OFF-Apex	68.11 \pm 0.32	54.22 \pm 0.36	67.66 \pm 0.30	67.03 \pm 0.27	79.22 \pm 0.25	78.5 \pm 0.23	-	-	-	-
Boost	-	-	68.89 \pm 0.31	68.1 \pm 0.39	-	-	70.92 \pm 0.30	71.90 \pm 0.30	62.84 \pm 0.35	63.23 \pm 0.31
DSSN	57.35 \pm 0.35	46.43 \pm 0.51	63.43 \pm 0.32	64.68 \pm 0.48	-	-	70.80 \pm 0.30	73.10 \pm 0.31	-	-
AU-GACN	70.24 \pm 0.30	43.33 \pm 0.34	-	-	80.26 \pm 0.33	80.10 \pm 0.21	71.22 \pm 0.29	35.54 \pm 0.39	-	-
Dynamic	-	-	76.10 \pm 0.28	71.01 \pm 0.35	81.80 \pm 0.26	77.00 \pm 0.30	72.61 \pm 0.28	67.09 \pm 0.30	65.18 \pm 0.32	65.15 \pm 0.36
MicroNet	74.11 \pm 0.28	73.64 \pm 0.48	76.80 \pm 0.28	74.45 \pm 0.45	80.59 \pm 0.32	81.79 \pm 0.32	75.61 \pm 0.29	70.12 \pm 0.30	-	-
Graph-TCN	75.00 \pm 0.28	69.93 \pm 0.37	77.46 \pm 0.27	76.19 \pm 0.45	79.61 \pm 0.39	84.11 \pm 0.40	74.08 \pm 0.29	72.58 \pm 0.32	67.43 \pm 0.26	68.73 \pm 0.39
FR	60.13 \pm 0.35	61.56 \pm 0.35	57.90 \pm 0.35	57.33 \pm 0.35	77.54 \pm 0.27	77.80 \pm 0.33	68.38 \pm 0.31	68.78 \pm 0.37	61.58 \pm 0.33	61.35 \pm 0.40
SelfME	69.43 \pm 0.28	70.22 \pm 0.31	-	-	75.25 \pm 0.30	74.66 \pm 0.19	74.55 \pm 0.29	76.30 \pm 0.29	71.01 \pm 0.22	69.77 \pm 0.25
FRL-DGT	-	-	73.08 \pm 0.32	72.01 \pm 0.32	78.00 \pm 0.26	79.13 \pm 0.22	75.12 \pm 0.30	76.58 \pm 0.22	70.11 \pm 0.25	70.56 \pm 0.25
MiMaNet	76.70 \pm 0.26	76.42 \pm 0.28	78.60 \pm 0.28	77.82 \pm 0.28	81.21 \pm 0.33	83.22 \pm 0.32	79.90 \pm 0.28	75.93 \pm 0.34	-	-
AMAN	68.85 \pm 0.31	66.83 \pm 0.31	79.87 \pm 0.27	77.14 \pm 0.31	-	-	75.40 \pm 0.28	71.33 \pm 0.34	67.45 \pm 0.32	66.49 \pm 0.43
μ -BERT	80.16 \pm 0.25	78.41 \pm 0.22	81.38 \pm 0.29	80.56 \pm 0.31	83.84 \pm 0.33	84.09 \pm 0.30	85.00 \pm 0.29	85.36 \pm 0.22	80.01 \pm 0.28	81.33 \pm 0.25
Meta-MMFNet	64.15 \pm 0.24	66.51 \pm 0.37	63.12 \pm 0.33	64.93 \pm 0.23	69.51 \pm 0.30	67.67 \pm 0.33	80.92 \pm 0.27	81.23 \pm 0.30	72.14 \pm 0.44	73.31 \pm 0.55
MEReMAML	74.23 \pm 0.30	76.37 \pm 0.31	80.78 \pm 0.24	81.51 \pm 0.32	78.12 \pm 0.30	79.56 \pm 0.28	86.21 \pm 0.20	89.26 \pm 0.21	76.12 \pm 0.29	75.89 \pm 0.18
LightmanNet	81.83 \pm 0.44	82.93 \pm 0.35	85.19 \pm 0.34	83.83 \pm 0.34	87.83 \pm 0.60	89.78 \pm 0.59	93.48 \pm 0.42	90.49 \pm 0.47	85.23 \pm 0.26	82.22 \pm 0.29

Table 2: Performance comparison (accuracy & F1 score \pm 95% confidence interval) of few-shot MER. The “*” denotes that the results are recorded on a subset instead of recorded via five rounds. See Appendix C for full results.

Method	SAMM(CK+)		SMIC(CK+)		CASME(CK+)		CASME II(CK+)		CAS(ME) ² (CK+)	
	ACC	F1								
MAML	59.00 \pm 0.00	61.00 \pm 0.00	58.00 \pm 0.00	57.00 \pm 0.00	64.00 \pm 0.00	61.00 \pm 0.00	63.00 \pm 0.00	60.00 \pm 0.00	59.00 \pm 0.00	62.00 \pm 0.00
Reptile	58.32 \pm 0.28	59.75 \pm 0.34	57.27 \pm 0.43	56.22 \pm 0.38	62.76 \pm 0.38	62.61 \pm 0.39	62.42 \pm 0.19	62.34 \pm 0.78	60.96 \pm 0.48	63.11 \pm 0.32
ANIL	57.47 \pm 0.37	62.42 \pm 0.39	-	-	64.53 \pm 0.33	61.97 \pm 0.12	-	-	58.84 \pm 0.32	62.76 \pm 0.34
ProtoNet	59.97 \pm 0.33	64.53 \pm 0.26	60.22 \pm 0.31	57.62 \pm 0.25	63.35 \pm 0.43	64.28 \pm 0.43	63.27 \pm 0.76	59.32 \pm 0.46	59.87 \pm 0.43	61.65 \pm 0.31
RelationNet	-	-	58.11 \pm 0.27	56.37 \pm 0.21	-	-	64.63 \pm 0.54	61.25 \pm 0.32	60.76 \pm 0.21	61.96 \pm 0.38
MatchingNet	61.42 \pm 0.36	59.51 \pm 0.32	60.46 \pm 0.34	58.79 \pm 0.38	65.43 \pm 0.76	61.74 \pm 0.35	62.54 \pm 0.35	61.45 \pm 0.76	-	-
Meta-MMFNet	64.15 \pm 0.24	66.51 \pm 0.37	63.12 \pm 0.33	64.93 \pm 0.23	69.5 \pm 0.30	67.67 \pm 0.33	80.92 \pm 0.27	81.23 \pm 0.30	72.14 \pm 0.44	73.31 \pm 0.55
MEReMAML	79.03 \pm 0.41	77.12 \pm 0.39	79.36 \pm 0.06*	81.23 \pm 0.19*	81.22 \pm 0.49	79.15 \pm 0.33	92.97 \pm 0.54	91.05 \pm 0.44	84.16 \pm 0.56	80.19 \pm 0.32
LightmanNet	81.83 \pm 0.44	82.93 \pm 0.35	85.19 \pm 0.34	83.83 \pm 0.34	87.83 \pm 0.60	89.78 \pm 0.59	93.48 \pm 0.42	90.49 \pm 0.47	85.23 \pm 0.26	82.22 \pm 0.29

or storage space required to store the model. All results reported are the averages of five independent runs.

5.2 Comparative Experiments

In this subsection, we introduce the comparative experiments conducted to evaluate the effectiveness of LightmanNet, including comparisons of performance and model efficiency.

Performance. We conduct comparison experiments about the performance of LightmanNet and all the baselines on five datasets mentioned in Subsection 5.1. We use consistent experimental settings for each baseline, including the backbone network, hardware platform, etc. The quantitative results are illustrated in Table 1 and Figure 4. From Table 1, we observe that LightmanNet achieves state-of-the-art (SOTA) accuracy and F1 score on all the benchmark

datasets. For example, LightmanNet reaches an accuracy of 81.83% in dataset SAMM, surpassing the second-best method by 5.13%, while achieving an improvement of more than 3% in both accuracy and F1 scores on CASME dataset. Furthermore, Figure 4 shows the UAR comparison results on the CDE dataset, which reflects the model performance on various tasks and domains. As expected, LightmanNet performs better than almost all the MER baselines. In summary, all the results demonstrate the outstanding effectiveness and robustness of our proposed method.

Model Efficiency. To ensure the effectiveness of the method in practical applications, we evaluate the model efficiency from three aspects: performance (accuracy %), training time (training hours, h), and model size (parameter size, M). Figure 5 shows the trade-off performance of various baselines and our LightmanNet. The horizontal

Table 3: Ablation study of LightmanNet on the CDE dataset, i.e., we analyze the impact of the three components of LightmanNet by activate or deactivate/replace the corresponding modules, including the feature extractor, the guidance of auxiliary task (the effect of introducing auxiliary tasks), and bi-level optimization. The “✓” indicates that the corresponding module is activated in the current experiment. We record the average results from five rounds of testing

Feature extractors	Conv4	✓	✓	✓			
	ResNet				✓		
	VGG-19					✓	
	DenseNet						✓
The guidance of auxiliary tasks	✓		✓	✓	✓	✓	✓
Bi-level optimization		✓	✓	✓	✓	✓	✓
ACC		80.15 ± 0.33	83.36 ± 0.38	91.10 ± 0.43	91.13 ± 0.36	91.05 ± 0.46	91.17 ± 0.39
F1		86.03 ± 0.37	86.59 ± 0.33	92.01 ± 0.42	91.96 ± 0.45	92.21 ± 0.33	92.09 ± 0.37
UAR		81.14 ± 0.33	83.77 ± 0.38	88.87 ± 0.49	88.91 ± 0.46	88.96 ± 0.33	89.15 ± 0.35

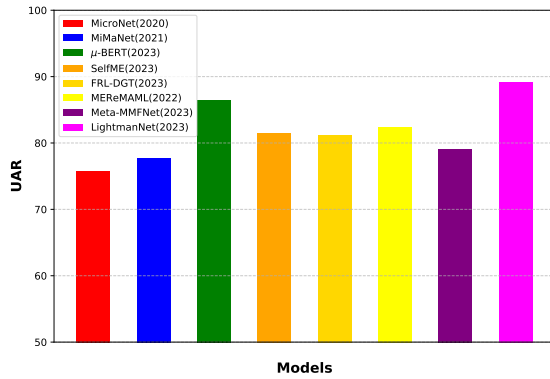


Figure 4: Performance comparison (UAR) of the baselines and our proposed LightmanNet on the CDE dataset. We choose the recently proposed baselines for comparison, which cover the SOTA and classic MER method on the CDE dataset, including meta-learning-based and deep-learning-based.

axis represents the training hours and the vertical axis represents the accuracy. The center of each circle represents the result of the training time and accuracy of each model, and the area of the circle represents the model size. From the results, we can observe that: (i) LightmanNet achieves performance far exceeding traditional MER methods with acceptable computation time and model size. (ii) Compared with the meta-learning-based and deep-learning-based baselines, LightmanNet achieves better results in a shorter time cost. The results demonstrate the outstanding model efficiency and advantages in real-world applications of LightmanNet.

5.3 Robust Analysis

Considering that the real-world MER faces problems of data scarcity and imbalanced class (one MER challenge mentioned in Section 1), we conduct robust analyses to evaluate the model’s performance on two challenging MER scenarios, i.e., the few-shot MER and MER with noises where the real-life applications will face.

Few-shot MER. To create few-shot tasks, we randomly choose K samples (each comprising M frames) from N classes, ensuring

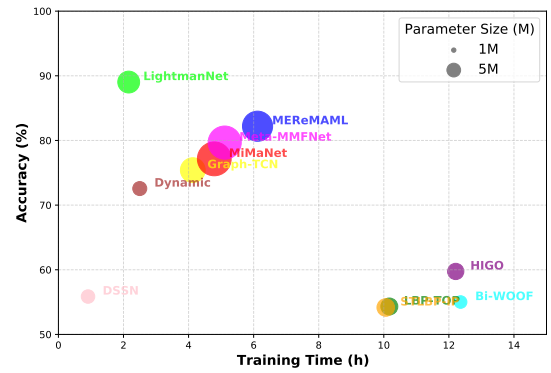


Figure 5: Model efficiency comparison of the baselines and LightmanNet on the CDE dataset, which is recorded with the same batch size and official code configuration. We record the performance of methods cover all the four types of baselines in Section 5.1 for 5 rounds of experiments.

no overlap between classes within each task. Here, $K = 1$ or $K = 5$ shows the meaning of few-shot learning, and each frame contains the label of macro-expressions and micro-expressions. This results in an N -way K -shot task, featuring N classes (different emotions of different individuals) and $N \times K$ samples. Before training, we construct N_{tr} training tasks through the above process and then train the model via the constructed training tasks. After training, we evaluate the trained model’s performance on unseen MER tasks by repeating the above random sampling process.

The results are shown in Table 2. From the results, we can observe that across almost all the datasets, LightmanNet consistently outperforms both meta-learning methods and MER methods. This indicates that LightmanNet can achieve similar or even superior generalization improvements compared to baselines, without the need for extensive data reliance in the real world.

MER with noises. In addition to data-level challenges, real-life MER also faces recognition difficulties caused by data quality, such as occlusion, low resolution [1, 35], etc. In order to verify the robustness of LightmanNet, we conduct experiments on the CDE

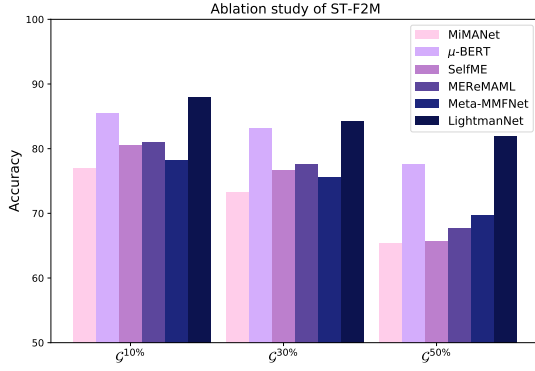


Figure 6: Performance comparison (Accuracy) on the CDE dataset when faces noises. The $\mathcal{G}^{10\%}$, $\mathcal{G}^{30\%}$, and $\mathcal{G}^{50\%}$ respectively represent samples faced with different proportions of noise, e.g., the results of $\mathcal{G}^{10\%}$ are the average results of three experiments on the CDE dataset with $\mathcal{P}_1^{10\%}$, $\mathcal{P}_2^{10\%}$, and $\mathcal{P}_3^{10\%}$.

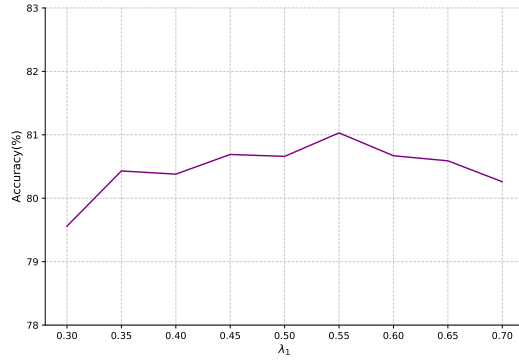


Figure 7: The ablation study of parametric sensitivity, i.e., the effect of hyperparameters λ_1 and λ_2 on model performance at different values. λ_1 and λ_2 are the hyperparameters of two branches' losses mentioned in Subsection 4. Note that $\lambda_2 = 1 - \lambda_1$, and the horizontal axis represents λ_1 .

dataset where the data are adjusted via three types of processing, i.e., introducing random mask \mathcal{P}_1 , introducing regional Gaussian noise \mathcal{P}_2 , and performing grayscale \mathcal{P}_3 . Then, we adjust the proportion of the adjusted data in the CDE dataset with 10%, 30%, and 50%, corresponding to the superscript of the operation \mathcal{P} , e.g., $\mathcal{P}_1^{10\%}$ denotes that 10% of the data with random masks. Next, we record the three sets of average results on different processing, e.g., the first set $\mathcal{G}^{10\%}$ denotes that recording the model performance on the CDE dataset with $\mathcal{P}_1^{10\%}$, $\mathcal{P}_2^{10\%}$, and $\mathcal{P}_3^{10\%}$.

The results are shown in Figure 6. From the results, we can observe that: (i) the performance of LightmanNet does not change much with all three scales of data corruption, proving its advantages in robustness; (ii) in particular, when the noise ratio reaches 50%, the performance of LightmanNet only drops less than 5%, significantly exceeding other methods. These findings verify the robustness and

effectiveness of LightmanNet and its advantages in practical applications, where data quality corruption due to acquisition difficulties of MER and artificial occlusion always exists.

5.4 Ablation Study

In this subsection, we conduct ablation studies to further explore how LightmanNet works. We first conduct experiments on the CDE dataset mentioned in Subsection 5.1 to evaluate the effect of different modules in LightmanNet. Next, we evaluate the parametric sensitivity of λ_1 and λ_2 , which are the hyperparameters of the two learning branches of LightmanNet.

The effect of different modules. We analyze the impact of the three components of LightmanNet, including the feature extractor, the guidance of auxiliary tasks (the effect of introducing auxiliary tasks), and bi-level optimization. We perform evaluation by activating or deactivating/replacing the corresponding modules. Specifically, for the feature extractor, we try four types of extractors, i.e., Conv4, ResNet, VGG-16, and DenseNet, as mentioned in Subsection 4.1. For the guidance of auxiliary tasks, we directly disabled the learning of auxiliary tasks and the model performs learning only through the primary branch. For the bi-level optimization, we replace our method with the traditional method but with the same encoder and use the common supervised learning manner, i.e., update the network only once per iteration. Table 3 shows the results. From the results, We can observe that: (i) for the feature extractors, their performance is not much different, and CONV4 is the lightest model which we choose as the extractor to improve efficiency. (ii) the dual-branch learning and bi-level optimization can effectively improve the model performance, achieving improvements higher than 5% and 7% respectively. This indicates that our design is foresighted.

Parametric Sensitivity. The hyperparameters λ_1 and λ_2 are the importance weights of two different branches of learning for the first-level optimization objective as mentioned in Eq.???. We evaluate the performance (accuracy(%)) of LightmanNet with different λ_1 and λ_2 , following the same implementation discussed in Subsection 5.2. Specifically, we vary λ_1 in the range of 0.3 ~ 0.7 where $\lambda_2 = 1 - \lambda_1$, and record the classification accuracy of Lightman using a Conv4 on SAMM dataset. The results are shown in Figure 7. We can observe that the model performance is optimal when $\lambda_1 = 0.55$ and $\lambda_2 = 0.45$, which are also the hyperparameter settings of LightmanNet.

6 CONCLUSION

In this paper, we explore three key challenges of micro-expression recognition in real-life applications together, i.e., data-level, feature-level, and decision-making-level issues, which have been ignored or limited in previous works. To address all the key challenges and perform well in the real world, we propose a novel dual-branch meta-auxiliary learning method, called LightmanNet, to achieve robust and fast micro-expression recognition. LightmanNet uses dual-branch bi-level optimization to learn general MER knowledge with limited data, which contains two steps: (i) in the first level, the model acquires two-branch knowledge for each task, where one branch handles the main MER task to learn MER features and the other branch performs an auxiliary task of magnifying and aligning micro-expressions and macro-expressions based on their similarity,

guiding the model obtain discriminative features; then (ii) in the second level, the model learn the general MER-related knowledge by refining the learned task-specific knowledge from multiple MER tasks, i.e., optimizing the model to make it perform well on various MER tasks. Extensive experiments on various benchmark datasets demonstrate the outstanding robustness and effectiveness of LightmanNet and its obvious advantages in real-world applications.

REFERENCES

- [1] Samar Al-Saqqa, Heba Abdel-Nabi, and Arafat Awajan. 2018. A survey of textual emotion detection. In *2018 8th International Conference on Computer Science and Information Technology (CSIT)*. IEEE, 136–142.
- [2] Yinbo Chen, Xiaolong Wang, Zhuang Liu, Huijuan Xu, Trevor Darrell, et al. 2020. A new meta-baseline for few-shot learning. *arXiv preprint arXiv:2003.04390*, 1, 2 (2020), 3.
- [3] Yuedong Chen, Xu Yang, Tat-Jen Cham, and Jianfei Cai. 2022. Towards unbiased visual emotion recognition via causal intervention. In *Proceedings of the 30th ACM International Conference on Multimedia*. 60–69.
- [4] Yi Dai and Ling Feng. 2021. Cross-domain few-shot micro-expression recognition incorporating action units. *IEEE Access* 9 (2021), 142071–142083.
- [5] Felicitas Datz, Guoruey Wong, and Henriette Löffler-Stastka. 2019. Interpretation and working through contemptuous facial micro-expressions benefits the patient-therapist relationship. *International Journal of Environmental Research and Public Health* 16, 24 (2019), 4901.
- [6] Adrian K Davison, Cliff Lansley, Nicholas Costen, Kevin Tan, and Moi Hoon Yap. 2016. Samm: A spontaneous micro-facial movement dataset. *IEEE transactions on affective computing* 9, 1 (2016), 116–129.
- [7] Pieter-Tjerk De Boer, Dirk P Kroese, Shie Mannor, and Reuven Y Rubinstein. 2005. A tutorial on the cross-entropy method. *Annals of operations research* 134 (2005), 19–67.
- [8] Paul Ekman. 2009. *Telling lies: Clues to deceit in the marketplace, politics, and marriage (revised edition)*. WW Norton & Company.
- [9] Xinqi Fan, Xueli Chen, Mingjie Jiang, Ali Raza Shahid, and Hong Yan. 2023. SelfME: Self-Supervised Motion Learning for Micro-Expression Recognition. In *Proceedings of the IEEE/CVF Conference on Computer Vision and Pattern Recognition*. 13834–13843.
- [10] Chelsea Finn, Pieter Abbeel, and Sergey Levine. 2017. Model-agnostic meta-learning for fast adaptation of deep networks. In *International conference on machine learning*. PMLR, 1126–1135.
- [11] Yee Siang Gan, Sze-Teng Liong, Wei-Chuen Yau, Yen-Chang Huang, and Lit-Ken Tan. 2019. OFF-ApexNet on micro-expression recognition system. *Signal Processing: Image Communication* 74 (2019), 129–139.
- [12] Spyros Gidaris and Nikos Komodakis. 2018. Dynamic few-shot visual learning without forgetting. In *Proceedings of the IEEE conference on computer vision and pattern recognition*. 4367–4375.
- [13] Wenjuan Gong, Yue Zhang, Wei Wang, Peng Cheng, and Jordi Gonzalez. 2023. Meta-MMFNet: Meta-learning-based multi-model fusion network for micro-expression recognition. *ACM Transactions on Multimedia Computing, Communications and Applications* 20, 2 (2023), 1–20.
- [14] SL Happy and Aurobinda Routray. 2017. Fuzzy histogram of optical flow orientations for micro-expression recognition. *IEEE Transactions on Affective Computing* 10, 3 (2017), 394–406.
- [15] Kaiming He, Xiangyu Zhang, Shaoqing Ren, and Jian Sun. 2016. Deep residual learning for image recognition. In *Proceedings of the IEEE conference on computer vision and pattern recognition*. 770–778.
- [16] Sepp Hochreiter, A Steven Younger, and Peter R Conwell. 2001. Learning to learn using gradient descent. In *Artificial Neural Networks—ICANN 2001: International Conference Vienna, Austria, August 21–25, 2001 Proceedings 11*. Springer, 87–94.
- [17] Timothy Hospedales, Antreas Antoniou, Paul Micaelli, and Amos Storkey. 2021. Meta-learning in neural networks: A survey. *IEEE transactions on pattern analysis and machine intelligence* 44, 9 (2021), 5149–5169.
- [18] Gao Huang, Zhuang Liu, Laurens Van Der Maaten, and Kilian Q Weinberger. 2017. Densely connected convolutional networks. In *Proceedings of the IEEE conference on computer vision and pattern recognition*. 4700–4708.
- [19] Xiaohua Huang, Su-Jing Wang, Guoying Zhao, and Matti Pietikäinen. 2015. Facial micro-expression recognition using spatiotemporal local binary pattern with integral projection. In *Proceedings of the IEEE international conference on computer vision workshops*. 1–9.
- [20] Xiaohua Huang, Guoying Zhao, Xiaopeng Hong, Wenming Zheng, and Matti Pietikäinen. 2016. Spontaneous facial micro-expression analysis using Spatiotemporal Completed Local Quantized Patterns. *Neurocomputing* (Jan 2016), 564–578. <https://doi.org/10.1016/j.neucom.2015.10.096>
- [21] Huai-Qian Khor, John See, Sze-Teng Liong, Raphael CW Phan, and Weiyao Lin. 2019. Dual-stream shallow networks for facial micro-expression recognition. In *2019 IEEE international conference on image processing (ICIP)*. IEEE, 36–40.
- [22] Sathish Kumar, Rama Prabha, and Selvakumar Samuel. 2022. Sentiment Analysis and Emotion Detection with Healthcare Perspective. In *Augmented Intelligence in Healthcare: A Pragmatic and Integrated Analysis*. Springer, 189–204.
- [23] Anh Cat Le Ngo, John See, and Raphael C-W Phan. 2016. Sparsity in dynamics of spontaneous subtle emotions: analysis and application. *IEEE Transactions on Affective Computing* 8, 3 (2016), 396–411.
- [24] Ling Lei, Jianfeng Li, Tong Chen, and Shigang Li. 2020. A novel graph-tcn with a graph structured representation for micro-expression recognition. In *Proceedings of the 28th ACM International Conference on Multimedia*. 2237–2245.
- [25] Juncheng Li, Junlin Xie, Linchao Zhu, Long Qian, Siliang Tang, Wenqiao Zhang, Haochen Shi, Shengyu Zhang, Longhui Wei, Qi Tian, et al. 2022. Dilated context integrated network with cross-modal consensus for temporal emotion localization in videos. In *Proceedings of the 30th ACM International Conference on Multimedia*. 5083–5092.
- [26] Rui Li, Yiting Wang, Wei-Long Zheng, and Bao-Liang Lu. 2022. A multi-view spectral-spatial-temporal masked autoencoder for decoding emotions with self-supervised learning. In *Proceedings of the 30th ACM International Conference on Multimedia*. 6–14.
- [27] Xiaobai Li, Xiaopeng Hong, Antti Moilanen, Xiaohua Huang, Tomas Pfister, Guoying Zhao, and Matti Pietikäinen. 2017. Towards reading hidden emotions: A comparative study of spontaneous micro-expression spotting and recognition methods. *IEEE transactions on affective computing* 9, 4 (2017), 563–577.
- [28] Xiaobai Li, Tomas Pfister, Xiaohua Huang, Guoying Zhao, and Matti Pietikäinen. 2013. A spontaneous micro-expression database: Inducement, collection and baseline. In *2013 10th IEEE International Conference and Workshops on Automatic face and gesture recognition (fg)*. IEEE, 1–6.
- [29] Sze-Teng Liong, Yee Siang Gan, John See, Huai-Qian Khor, and Yen-Chang Huang. 2019. Shallow triple stream three-dimensional cnn (ststnet) for micro-expression recognition. In *2019 14th IEEE international conference on automatic face & gesture recognition (FG 2019)*. IEEE, 1–5.
- [30] Sze-Teng Liong, John See, KokSheik Wong, and Raphael C-W Phan. 2018. Less is more: Micro-expression recognition from video using apex frame. *Signal Processing: Image Communication* 62 (2018), 82–92.
- [31] Huan Liu, Zhixiang Chi, Yuanhao Yu, Yang Wang, Jun Chen, and Jin Tang. 2023. Meta-Auxiliary Learning for Future Depth Prediction in Videos. In *Proceedings of the IEEE/CVF Winter Conference on Applications of Computer Vision*. 5756–5765.
- [32] Yong-Jin Liu, Jin-Kai Zhang, Wen-Jing Yan, Su-Jing Wang, Guoying Zhao, and Xiaolan Fu. 2016. A Main Directional Mean Optical Flow Feature for Spontaneous Micro-Expression Recognition. *IEEE Transactions on Affective Computing* (Oct 2016), 299–310. <https://doi.org/10.1109/taffc.2015.2485205>
- [33] Hua Lu, Kidiyo Kpalma, and Joseph Ronsin. 2018. Motion descriptors for micro-expression recognition. *Signal Processing: Image Communication* 67 (2018), 108–117.
- [34] Walied Merghani, Adrian K Davison, and Moi Hoon Yap. 2018. A review on facial micro-expressions analysis: datasets, features and metrics. *arXiv preprint arXiv:1805.02397* (2018).
- [35] Elham Naji Meidani, Hossein Makiabadi, Mohammad Zabetipour, Hannaneh Abbasnejad, Aida Firoozian Pooresefehni, and Shaghayegh Shayesteh. 2022. Emo-Sensory Communication, Emo-Sensory Intelligence and Gender. *Journal of Business, Communication & Technology* 1, 2 (2022), 54–66.
- [36] Borum Nam, Joo Young Kim, Beomjun Bark, Yeongmyeong Kim, Jiyeon Kim, Soon Won So, Hyung Youn Choi, and In Young Kim. 2023. FacialCueNet: unmasking deception-an interpretable model for criminal interrogation using facial expressions. *Applied Intelligence* 53, 22 (2023), 27413–27427.
- [37] Aviv Navon, Idan Achituve, Haggai Maron, Gal Chechik, and Ethan Fetaya. 2020. Auxiliary learning by implicit differentiation. *arXiv preprint arXiv:2007.02693* (2020).
- [38] Bernhard Nebel. 2000. On the compilability and expressive power of propositional planning formalisms. *Journal of Artificial Intelligence Research* 12 (2000), 271–315.
- [39] Xuan-Bac Nguyen, Chi Nhan Duong, Xin Li, Susan Gauch, Han-Seok Seo, and Khoa Luu. 2023. Micron-BERT: BERT-based Facial Micro-Expression Recognition. In *Proceedings of the IEEE/CVF Conference on Computer Vision and Pattern Recognition*. 1482–1492.
- [40] Alex Nichol and John Schulman. 2018. Reptile: a scalable metalearning algorithm. *arXiv preprint arXiv:1803.02999* 2, 3 (2018), 4.
- [41] Jicai Pan and Shangfei Wang. 2023. Progressive Visual Content Understanding Network for Image Emotion Classification. In *Proceedings of the 31st ACM International Conference on Multimedia*. 6034–6044.
- [42] Wei Peng, Xiaopeng Hong, Yingyue Xu, and Guoying Zhao. 2019. A boost in revealing subtle facial expressions: A consolidated eulerian framework. In *2019 14th IEEE International Conference on Automatic Face & Gesture Recognition (FG 2019)*. IEEE, 1–5.
- [43] Siyuan Qiao, Chenxi Liu, Wei Shen, and Alan L Yuille. 2018. Few-shot image recognition by predicting parameters from activations. In *Proceedings of the IEEE conference on computer vision and pattern recognition*. 7229–7238.

- [44] Fangbing Qu, Su-Jing Wang, Wen-Jing Yan, He Li, Shuhang Wu, and Xiaolan Fu. 2018. CAS (ME)-: A Database for Spontaneous Macro-Expression and Micro-Expression Spotting and Recognition. *IEEE Transactions on Affective Computing* 9, 04 (2018), 424–436.
- [45] Aniruddh Raghu, Maithra Raghu, Samy Bengio, and Oriol Vinyals. 2019. Rapid learning or feature reuse? towards understanding the effectiveness of maml. *arXiv preprint arXiv:1909.09157* (2019).
- [46] Sachin Ravi and Hugo Larochelle. 2016. Optimization as a model for few-shot learning. In *International conference on learning representations*.
- [47] Olaf Ronneberger, Philipp Fischer, and Thomas Brox. 2015. U-net: Convolutional networks for biomedical image segmentation. In *Medical Image Computing and Computer-Assisted Intervention—MICCAI 2015: 18th International Conference, Munich, Germany, October 5–9, 2015, Proceedings, Part III* 18. Springer, 234–241.
- [48] Adam Santoro, Sergey Bartunov, Matthew Botvinick, Daan Wierstra, and Timothy Lillicrap. 2016. Meta-learning with memory-augmented neural networks. In *International conference on machine learning*. PMLR, 1842–1850.
- [49] Karen Simonyan and Andrew Zisserman. 2014. Very deep convolutional networks for large-scale image recognition. *arXiv preprint arXiv:1409.1556* (2014).
- [50] Jake Snell, Kevin Swersky, and Richard Zemel. 2017. Prototypical networks for few-shot learning. *Advances in neural information processing systems* 30 (2017).
- [51] Bo Sun, Siming Cao, Dongliang Li, Jun He, and Lejun Yu. 2020. Dynamic micro-expression recognition using knowledge distillation. *IEEE Transactions on Affective Computing* 13, 2 (2020), 1037–1043.
- [52] Flood Sung, Yongxin Yang, Li Zhang, Tao Xiang, Philip HS Torr, and Timothy M Hospedales. 2018. Learning to compare: Relation network for few-shot learning. In *Proceedings of the IEEE conference on computer vision and pattern recognition*. 1199–1208.
- [53] Richard Szeliski et al. 2007. Image alignment and stitching: A tutorial. *Foundations and Trends® in Computer Graphics and Vision* 2, 1 (2007), 1–104.
- [54] Oriol Vinyals, Charles Blundell, Timothy Lillicrap, Daan Wierstra, et al. 2016. Matching networks for one shot learning. *Advances in neural information processing systems* 29 (2016).
- [55] Bo Wan, Junjun Dang, Xuanxuan Liu, and Qi Wang. 2022. Micro-Expression Recognition Based on MAML Meta-Learning Algorithm. In *2022 IEEE Smartworld, Ubiquitous Intelligence & Computing, Scalable Computing & Communications, Digital Twin, Privacy Computing, Metaverse, Autonomous & Trusted Vehicles (SmartWorld/UIC/ScalCom/DigitalTwin/PriComp/Meta)*. IEEE, 1322–1328.
- [56] Jingyao Wang, Luntian Mou, Lei Ma, Tiejun Huang, and Wen Gao. 2023. AMSA: adaptive multimodal learning for sentiment analysis. *ACM Transactions on Multimedia Computing, Communications and Applications* 19, 3s (2023), 1–21.
- [57] Lijuan Wang, Guoli Jia, Ning Jiang, Haiying Wu, and Jufeng Yang. 2022. Ease: Robust facial expression recognition via emotion ambiguity-sensitive cooperative networks. In *Proceedings of the 30th ACM International Conference on Multimedia*. 218–227.
- [58] Yandan Wang, John See, Raphael C-W Phan, and Yee-Hui Oh. 2015. Lbp with six intersection points: Reducing redundant information in lbp-top for micro-expression recognition. In *Computer Vision—ACCV 2014: 12th Asian Conference on Computer Vision, Singapore, Singapore, November 1–5, 2014, Revised Selected Papers, Part I* 12. Springer, 525–537.
- [59] Mengting Wei, Wenming Zheng, Yuan Zong, Xingxun Jiang, Cheng Lu, and Jiateng Liu. 2022. A novel micro-expression recognition approach using attention-based magnification-adaptive networks. In *ICASSP 2022-2022 IEEE International Conference on Acoustics, Speech and Signal Processing (ICASSP)*. IEEE, 2420–2424.
- [60] Bin Xia and Shangfei Wang. 2021. Micro-Expression Recognition Enhanced by Macro-Expression from Spatial-Temporal Domain. In *IJCAI* 1186–1193.
- [61] Bin Xia, Weikang Wang, Shangfei Wang, and Enhong Chen. 2020. Learning from macro-expression: a micro-expression recognition framework. In *Proceedings of the 28th ACM International Conference on Multimedia*. 2936–2944.
- [62] Hong-Xia Xie, Ling Lo, Hong-Han Shuai, and Wen-Huang Cheng. 2020. Au-assisted graph attention convolutional network for micro-expression recognition. In *Proceedings of the 28th ACM International Conference on Multimedia*. 2871–2880.
- [63] Wen-Jing Yan, Xiaobai Li, Su-Jing Wang, Guoying Zhao, Yong-Jin Liu, Yu-Hsin Chen, and Xiaolan Fu. 2014. CASME II: An improved spontaneous micro-expression database and the baseline evaluation. *PLoS one* 9, 1 (2014), e86041.
- [64] Wen-Jing Yan, Qi Wu, Yong-Jin Liu, Su-Jing Wang, and Xiaolan Fu. 2013. CASME database: A dataset of spontaneous micro-expressions collected from neutralized faces. In *2013 10th IEEE international conference and workshops on automatic face and gesture recognition (FG)*. IEEE, 1–7.
- [65] Dingkan Yang, Shuai Huang, Haopeng Kuang, Yangtao Du, and Lihua Zhang. 2022. Disentangled representation learning for multimodal emotion recognition. In *Proceedings of the 30th ACM International Conference on Multimedia*. 1642–1651.
- [66] Zhijun Zhai, Jianhui Zhao, Chengjiang Long, Wenju Xu, Shuangjiang He, and Huijuan Zhao. 2023. Feature Representation Learning with Adaptive Displacement Generation and Transformer Fusion for Micro-Expression Recognition. In *Proceedings of the IEEE/CVF Conference on Computer Vision and Pattern Recognition*. 22086–22095.
- [67] Jiawei Zhang, Zizhao Dong, and Su-Jing Wang. 2023. Micro Expression Recognition by Machine Learning Based Profit Function Analysis in Intelligent Marketing of Financial Industry. In *2023 IEEE 6th Eurasian Conference on Educational Innovation (ECEI)*. IEEE, 188–192.
- [68] Liang Zhang, Guangming Zhu, Peiyi Shen, Juan Song, Syed Afaq Shah, and Mohammed Bennamoun. 2017. Learning spatiotemporal features using 3dcnn and convolutional lstm for gesture recognition. In *Proceedings of the IEEE international conference on computer vision workshops*. 3120–3128.
- [69] Guoying Zhao and Matti Pietikainen. 2007. Dynamic Texture Recognition Using Local Binary Patterns with an Application to Facial Expressions. *IEEE Transactions on Pattern Analysis and Machine Intelligence* (Jun 2007), 915–928. <https://doi.org/10.1109/tpami.2007.1110>
- [70] Ling Zhou, Qirong Mao, Xiaohua Huang, Feifei Zhang, and Zhihong Zhang. 2022. Feature refinement: An expression-specific feature learning and fusion method for micro-expression recognition. *Pattern Recognition* 122 (2022), 108275.
- [71] Ling Zhou, Xiuyan Shao, and Qirong Mao. 2021. A survey of micro-expression recognition. *Image and Vision Computing* 105 (2021), 104043.